

Measuring the local pressure amplitude in microchannel acoustophoresis

Rune Barnkob,^a Per Augustsson,^b Thomas Laurell^b and Henrik Bruus^{*a}

Received 1st October 2009, Accepted 7th December 2009

First published as an Advance Article on the web 27th January 2010

DOI: 10.1039/b920376a

A new method is reported on how to measure the local pressure amplitude and the Q factor of ultrasound resonances in microfluidic chips designed for acoustophoresis of particle suspensions. The method relies on tracking individual polystyrene tracer microbeads in straight water-filled silicon/glass microchannels. The system is actuated by a PZT piezo transducer attached beneath the chip and driven by an applied ac voltage near its eigenfrequency of 2 MHz. For a given frequency a number of particle tracks are recorded by a CCD camera and fitted to a theoretical expression for the acoustophoretic motion of the microbeads. From the curve fits we obtain the acoustic energy density, and hence the pressure amplitude as well as the acoustophoretic force. By plotting the obtained energy densities as a function of applied frequency, we obtain Lorentzian line shapes, from which the resonance frequency and the Q factor for each resonance peak are derived. Typical measurements yield acoustic energy densities of the order of 10 J/m³, pressure amplitudes of 0.2 MPa, and Q factors around 500. The observed half wavelength of the transverse acoustic pressure wave is equal within 2% to the measured width $w = 377 \mu\text{m}$ of the channel.

I. Introduction

The studies of acoustic radiation forces on particles have a long history. The analysis of incompressible particles in acoustic fields dates back to the work in 1934 by King,¹ while the forces on compressible particles was calculated in 1955 by Yosioka and Kawasima.² Their work was admirably summarized and generalized in 1962 in a short paper by Gorkov.³ The use of ultrasound standing waves for particle manipulation and separation has received renewed interest in the past decade as represented by the early papers ref. 4–6, which demonstrate this possibility.

The subsequent transition to a microscale format, where the acoustic resonators were tuned to match a half wavelength or a few multiples thereof, has boosted the ability to more precisely control the localization of cells and particles by acoustic forces. In their seminal paper,⁷ Hawkes *et al.* presented a first precision machined half-wavelength resonator for continuous flow focusing of particles, and Nilsson *et al.* demonstrated early the ability to trap particles in quartz capillaries performing a bead based immuno assay.⁸ This was followed by improved fabrication conditions by silicon/glass microfabrication technologies, which opened the route to lab-on-a-chip integration of ultrasonic standing wave technology, where both acoustic trapping and continuous flow separations have emerged as two major application areas in biomedical research as reviewed in ref. 9 and 10.

The method of acoustic particle trapping has subsequently undergone a rapid development, and it is now used in several different microchip configurations.^{11–16} Likewise, the development of continuous-flow-based separation and manipulation of particles and cells has progressed rapidly with the advent of

precision microfabricated flow-through resonators operating in the laminar flow regime.^{17–26} Both the area of acoustic trapping and continuous separation/manipulation show great promise for applications within flow cytometry, and much of the current technological development targets cell biology.

In parallel, intense efforts are made to find physical models which fully describe the resonance modes of the microchips, such that up-front design can be made by numerical simulation. Along this line Benes, Hill, Hawkes and co-workers were early in outlining models for the treatment of the two dimensional layered acoustic resonator.^{27–31} Lately, it has proven useful to model resonant microchannel or microcavity lab-on-a-chip systems by the Helmholtz pressure-wave eigenvalue equation for the actual chip geometries. In the 2D-limit, *i.e.* when the chip thickness is smaller than a half wavelength, the resulting pressure eigenmodes display close resemblance with the experimental conditions.^{32,33} However, although these simulations describe the resonance modes, they do not indicate the magnitude of the Q factor or the line width of the modes.

This is also reflected in the key problem of the application of standing ultrasound waves in microfluidic systems, namely the prediction and measurement of the absolute size of the acoustophoretic force and the pressure amplitude acting on suspended particles or cells. Acoustic power sent from the transducer to the microfluidic system suffers losses due to thermal dissipation in the piezo-ceramic transducer, and acoustic radiation losses to the surroundings. These losses often vary from experiment to experiment and are thus difficult to estimate. At the same time there are no reliable methods available that enable the direct measurement of the pressure amplitude inside the microchannel without perturbing the microsystem severely or relying on external electric³⁴ or gravitational¹⁴ fields. Linking these experimental acoustic parameters to the theoretical modeling is currently not a viable route.

In this paper we present a novel method to measure the acoustic energy density and pressure amplitude acting on suspended

^aDepartment of Micro- and Nanotechnology, Technical University of Denmark, DTU Nanotech Building 345 East, DK-2800 Kongens Lyngby, Denmark. E-mail: Henrik.Bruus@nanotech.dtu.dk

^bDepartment of Electrical Measurements, Lund University, Box 118, S-221 00 Lund, Sweden

microbeads undergoing acoustophoresis. Also, we experimentally determine the acoustophoretic force on the microbeads and the Q factor of the associated ultrasonic standing wave resonance. The experimental method relies on tracking individual microbeads at a given ultrasound frequency, as they by acoustophoresis traverse the microchannel towards their equilibrium position at the center of the channel. The measured trajectories are fitted to a theoretical prediction derived from the expression for the force^{2,3} containing the acoustic energy density as a fitting parameter. By plotting the obtained energy density as a function of applied frequency we can also determine the pressure amplitude, the resonance frequency and the Q factor of the associated ultrasound resonance by fitting the resonance spectra to a sum of Lorentzian response curves.

II. Background theory

Linear acoustics and acoustic radiation forces are treated in many textbooks. Basic theory is presented in the textbook by Lighthill³⁵ and theoretical aspects of acoustics in microfluidics, termed acoustofluidics, can be found in the textbook by Bruus.³⁶ In this work we rely on the formulation of microbead acoustophoresis by Gorkov.³

A. Governing equations and boundary conditions

We consider a silicon/glass chip containing a microchannel filled with an aqueous suspension of particles. A piezo transducer is attached to the chip, such that when applying an ac voltage at MHz frequency, the piezo element vibrates and induces a time-harmonic ultrasound pressure field $p_1 \exp(-i\omega t)$, where $\omega = 2\pi f$ is the angular frequency and f the frequency. Here, we use the complex representation of the harmonic time dependence. In the following the time-harmonic factor is implicitly assumed. Likewise for the velocity field \mathbf{v}_1 of the carrier liquid.

Before the onset of the external ultrasound field the suspension is in a quiescent state at constant uniform pressure and zero velocity. The viscosity of the carrier liquid has a negligible influence on the acoustic radiation forces. Consequently, to a good approximation, the pressure field p_1 and velocity field \mathbf{v}_1 inside the chip and the microchannel are governed by simple linear acoustics of inviscid fluids, *i.e.* the Helmholtz wave equation for the pressure and potential flow for the velocity,

$$\nabla^2 p_1 = -\frac{\omega^2}{c^2} p_1, \quad (1a)$$

$$\mathbf{v}_1 = -\frac{i}{\omega\rho} \nabla p_1. \quad (1b)$$

Here, c and ρ are the speed of sound and the density of the given material, respectively. Note that in this simple qualitative model we neglect the shear waves in the solids, and in the following c_{si} and c_{py} are taken to be the longitudinal sound velocities representing the elastic behavior in silicon and pyrex glass, respectively, see Table 1.

The time-averaged acoustic energy density E_{ac}^{3D} can be expressed in terms of p_1 as follows,³⁶

$$E_{\text{ac}}^{3D} = \frac{1}{4\rho_{\text{wa}}} \left[\frac{|\nabla p_1|^2}{\omega^2} + \frac{p_1^2}{c_{\text{wa}}^2} \right]. \quad (2)$$

Table 1 Physical parameters used in the acoustic model

Speed of sound, water	c_{wa}	1483 m s ⁻¹
Speed of sound, silicon	c_{si}	8490 m s ⁻¹
Speed of sound, pyrex glass	c_{py}	5647 m s ⁻¹
Speed of sound, polystyrene	c_{ps}	1700 m s ⁻¹
Density, water	ρ_{wa}	998 kg m ⁻³
Density, silicon	ρ_{si}	2331 kg m ⁻³
Density, pyrex glass	ρ_{py}	2230 kg m ⁻³
Density, polystyrene	ρ_{ps}	1050 kg m ⁻³
Sound speed ratio $c_{\text{ps}}/c_{\text{wa}}$	β_{ps}	1.15
Density ratio $\rho_{\text{ps}}/\rho_{\text{wa}}$	γ_{ps}	1.05
Compressibility factor, polystyrene/water	f_1	0.276
Density factor, polystyrene/water	f_2	0.034
Acoustophoretic coefficient, polystyrene/water	Φ_{ps}	0.328

Henceforth, we only consider time-averaged energy densities.

In this work, at a boundary with surface normal vector \mathbf{n} , we employ one of the following three boundary conditions: the hard wall (zero velocity) condition, the soft wall (zero pressure) condition, and the continuity condition for pressure and velocity across interior boundaries,

$$\mathbf{n} \cdot \nabla p_1 = 0, \text{ (hard wall)}, \quad (3a)$$

$$p_1 = 0, \text{ (soft wall)}, \quad (3b)$$

$$\frac{\mathbf{n} \cdot \nabla p_1^{(a)}}{\rho_a} = \frac{\mathbf{n} \cdot \nabla p_1^{(b)}}{\rho_b}, \text{ and } p_1^{(a)} = p_1^{(b)}, \text{ (continuity)}. \quad (3c)$$

Products of these first-order acoustic fields give rise to two second-order effects, which persist even after time averaging: The acoustic radiation force acting on particles in suspension, and the acoustic streaming acting on the carrier liquid itself. As discussed in Section II D, the radiation force is the only second-order effect of importance in this work.

B. Acoustic resonances

The acoustically soft water inside the channel surrounded by the acoustically hard silicon/glass chip forms an acoustic cavity. This implies that acoustic resonances occur for certain specific frequencies $\omega_j, j = 1, 2, 3, \dots$. An acoustic resonance at frequency ω_j is a state where the average acoustic energy density inside the cavity is several orders of magnitude larger than at other frequencies $\omega \neq \omega_j$. By tuning the applied frequency to one of these resonance frequencies, the acoustic forces become so strong that they, in a reliable way, can be used to manipulate particles suspended in the carrier liquid.

The exact values of the resonance frequencies ω_j depend on the geometry of the acoustic cavity and of the material parameters of the liquid in the cavity as well as the surrounding material. Specifically, the relevant material parameters are the speed of sound c_{wa} and density ρ_{wa} of the water and likewise the speed of sound c_{si} and density ρ_{si} of the silicon chip, see Table 1. In the general case, the resonance frequencies can only be calculated using numerical methods.

For a rectangular channel of length l , width w , and height h , surrounded by an acoustically infinitely hard material, the resonance frequencies may be found analytically. This case approximates our experimental system reasonably well if we disregard the inlet and outlet of the microchannel. Moreover,

since the parameters listed in Table 1 yield an acoustic impedance ratio $(\rho_{\text{si}}c_{\text{si}})/(\rho_{\text{wa}}c_{\text{wa}}) = 13.4$ much larger than unity, the silicon surrounding our rectangular water channel can to a good approximation be treated as an infinitely hard material. In that case the normal velocity on all walls is zero, which according to eqn (1b) is equivalent to Neumann boundary conditions $\mathbf{n} \cdot \nabla p_1 = 0$ for the pressure. It is easily verified that with this boundary condition the pressure p_1 solving eqn (1a) for a rectangular box placed along the coordinate axes with its opposite corners at $(0, 0, 0)$ and (l, w, h) is

$$p_1(x, y, z) = p_a \cos(k_x x) \cos(k_y y) \cos(k_z z) \quad (4)$$

where p_a is the pressure amplitude, and $(k_x, k_y, k_z) = \pi(n_x/l, n_y/w, n_z/h)$ with $n_x, n_y, n_z = 0, 1, 2, \dots$. The corresponding three-index resonance frequencies $f_{n_x, n_y, n_z} = \omega_{n_x, n_y, n_z}/(2\pi)$ are given by

$$f_{n_x, n_y, n_z} = \frac{c_{\text{wa}}}{2} \sqrt{\frac{n_x^2}{l^2} + \frac{n_y^2}{w^2} + \frac{n_z^2}{h^2}} \quad (5)$$

with $n_x, n_y, n_z = 0, 1, 2, \dots$

For later use we denote the transverse wavelength in the y -direction by λ . The lowest resonance condition in this direction is thus $w = \lambda/2$ or $k_y = \pi/w$. Two examples of resonant standing ultrasound waves are shown in Fig. 1.

C. The acoustic radiation force

Given the pressure field p_1 and velocity field \mathbf{v}_1 it is possible to calculate the acoustic radiation force on a particle with volume $V = (4\pi/3)a^3$ and radius a much smaller than the acoustic wavelength λ . Both for biological cells and for microbeads used as tracers we are in this limit. The material parameters, with subscripts “wa” for the water and “p” for the particle, enter as the speed of sound ratio β and the density ratio γ ,

$$\beta = \frac{c_p}{c_{\text{wa}}}, \quad \gamma = \frac{\rho_p}{\rho_{\text{wa}}} \quad (6)$$

which appear in the compressibility factor f_1 and the density factor f_2 as

$$f_1 = 1 - \frac{1}{\gamma\beta^2}, \quad f_2 = \frac{2\gamma - 2}{2\gamma + 1}. \quad (7)$$

The general expression for the time-averaged acoustic radiation force $\langle \mathbf{F}_{\text{ac}} \rangle$ is a gradient of a potential,³

$$\langle \mathbf{F}_{\text{ac}} \rangle = -\nabla U_{\text{ac}}, \quad (8)$$

where this acoustic potential U_{ac} is given by

$$U_{\text{ac}} = V \left[\frac{f_1}{2\rho_{\text{wa}}c_{\text{wa}}^2} \langle p_1^2 \rangle - \frac{3f_2\rho_{\text{wa}}}{4} \langle |\mathbf{v}_1|^2 \rangle \right] \quad (9)$$

$$= \frac{V}{4\rho_{\text{wa}}c_{\text{wa}}^2} \left[2f_1 \langle p_1^2 \rangle - 3f_2 \frac{1}{k^2} \langle |\nabla p_1|^2 \rangle \right].$$

The latter form is obtained by use of eqn (1b) and $k^2 = k_x^2 + k_y^2 + k_z^2$.

To a good approximation the pressure eigenmodes p_1 are given by simple cosine/sine standing waves in a water channel surrounded by infinitely hard walls. For $h < w, l$, the pressure eigenmode eqn (4) can be approximated by the 2D expression with $k_z = 0$,

$$p_1(x, y, z) = p_a \cos(k_x x) \cos(k_y y), \quad (10a)$$

$$\nabla p_1(x, y, z) = -k_x p_a \sin(k_x x) \cos(k_y y) \mathbf{e}_x - k_y p_a \cos(k_x x) \sin(k_y y) \mathbf{e}_y. \quad (10b)$$

This standing wave can be interpreted as two counter-propagating waves along the direction $\mathbf{k} = k_x \mathbf{e}_x + k_y \mathbf{e}_y$, which forms the angle θ with the x -axis,

$$\cos \theta = \frac{k_x}{k}, \quad \sin \theta = \frac{k_y}{k}, \quad k = \sqrt{k_x^2 + k_y^2}. \quad (11)$$

Inserting this in Gorkov’s expression, eqn (9), we arrive at the acoustic potential

$$U_{\text{ac}} = U_o [2f_1 \cos^2(k_x x) \cos^2(k_y y) - 3f_2 \sin^2(k_x x) \cos^2(k_y y) \cos^2 \theta - 3f_2 \cos^2(k_x x) \sin^2(k_y y) \sin^2 \theta] \quad (12)$$

with an amplitude U_o given by

$$U_o = \frac{p_a^2 V}{8\rho_{\text{wa}}c_{\text{wa}}^2} = \frac{2\pi}{3} a^3 E_{\text{ac}}, \quad (13)$$

where $E_{\text{ac}} = p_a^2/(4\rho_{\text{wa}}c_{\text{wa}}^2)$ is the position-independent acoustic energy density for a 1D standing wave derived from eqn (2). A numerical example of the acoustic potential U_{ac}/U_o for a polystyrene sphere is shown in Fig. 2. Similar plots are found in refs. 37 and 38.

For later use we state the position-dependent acoustic energy density E_{ac}^{2D} for the 2D standing wave given in eqn (10a):

$$E_{\text{ac}}^{2D}(x, y) = [\sin^2 \theta \cos^2(k_x x) + \cos^2 \theta \cos^2(k_y y)] E_{\text{ac}}. \quad (14)$$

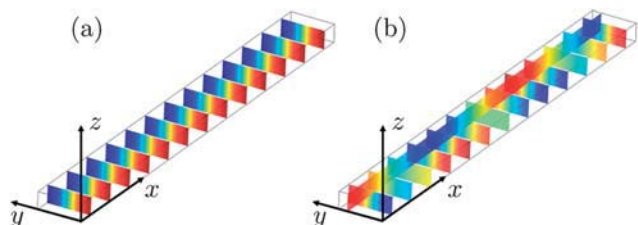


Fig. 1 Color plot (red positive, blue negative) of the pressure field p_1 at resonance in a water-filled microchannel of length $l = 40$ mm along x , width $w = 377$ μm along y , and height $h = 157$ μm along z , surrounded by an infinitely hard acoustic material, see eqn (4). (a) Resonance $(n_x, n_y, n_z) = (0, 1, 0)$ with $f_{0,1,0} = 1.9668$ MHz, and (b) $(n_x, n_y, n_z) = (3, 1, 0)$ with $f_{3,1,0} = 1.9676$ MHz.

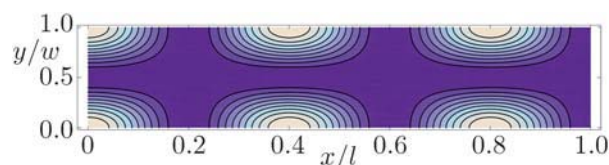


Fig. 2 Contour plot with 10% contour lines from low (dark) to high (light) of the normalized acoustic potential U_{ac}/U_o from eqn (12) for a polystyrene sphere in water given the pressure field p_1 of eqn (10a) with $(k_x, k_y) = (\pi/(2w), \pi/l)$ so that $\theta \approx 63^\circ$. Further parameter values used in the simulation are given in Table 1.

D. Transverse particle path

The path of a microbead moving under acoustophoresis is given by the position vector $(x(t), y(t))$. A particularly simple analytical expression for the transverse part $y(t)$ of this path can be obtained from eqn (8) and (12) in the limit of a long axial wavelength, $k_x \approx 0$, *i.e.* a 1D transverse wave. Given this, the y -component F_y of the acoustophoretic force becomes

$$F_y = 2k_y U_o \left[\frac{5\gamma - 2}{2\gamma + 1} - \frac{1}{\gamma\beta^2} \right] \sin(2k_y y). \quad (15)$$

We can neglect inertial effects because the flow speed of our 5- μm -microbeads never exceeds 200 $\mu\text{m}/\text{s}$ resulting in a Reynolds number less than 0.001. We can also neglect the influence from the Stokes drag due to the acoustic streaming. This was demonstrated experimentally by Hagsäter *et al.*³² In a direct comparison of the acoustic forces on microbeads in a microfluidic chamber it was shown that the motion of 1 μm beads was governed entirely by Stokes drag from the acoustic streaming, while the motion of the 5 μm beads was dominated by the acoustic radiation force. Moreover, in this work we never observed any traces of acoustic flow rolls.

To determine the transverse path $y(t)$ we therefore balance the acoustophoretic force F_y with the Stokes drag force due to the viscosity η from the quiescent liquid, and obtain the following differential equation,

$$6\pi\eta a \frac{dy}{dt} = 2k_y U_o \Phi \sin(2k_y y) \quad (16)$$

where Φ is the acoustophoretic coefficient,³⁹

$$\Phi = \frac{5\gamma - 2}{2\gamma + 1} - \frac{1}{\gamma\beta^2} \quad (17)$$

Separating the variables y and t , and using the fact that $2 \int ds / \sin(2s) = \log|\tan(s)|$ leads to an analytical expression for the transverse path

$$y(t) = \frac{1}{k_y} \arctan \left\{ \tan[k_y y(0)] \exp \left[\frac{4\Phi}{9\eta} (k_y a)^2 E_{ac} t \right] \right\} \quad (18)$$

where $y(0)$ is the transverse position at time $t = 0$. Such paths have previously been calculated numerically by Townsend *et al.*⁴⁰

Inverting the above expression, we can also calculate the time t it takes for a particle to move from any initial position $y(0)$ to any final position $y(t)$,

$$t = \frac{9\eta}{4\Phi (k_y a)^2 E_{ac}} \ln \left[\frac{\tan[k_y y(t)]}{\tan[k_y y(0)]} \right] \quad (19)$$

A special case of this expression, namely the time for a particle to reach the nodal line, was derived by Limaye and Coakley.⁴¹

E. Resonance line shape

It is straightforward to show that the acoustic energy density $E_{ac}(f)$ for a liquid slab between two walls counter-oscillating at frequency f exhibits a Lorentzian line shape near any given resonance frequency f_1 ,

$$E_{ac}(f) = \frac{E_1}{\left[\frac{2Q_1}{f_1} (f - f_1) \right]^2 + 1} \quad (20)$$

The maximum of the energy density at resonance is E_1 , while the full-width at half-maximum is $\delta f_1 = f_1/Q_1$, where the Q factor Q_1 of the resonance is related to dissipation of the acoustic energy due to viscosity in the bulk liquid and radiation losses from the surfaces of the chip.

III. Chip, setup, and experimental procedure

A. Chip and experimental setup

To study the local acoustic pressure amplitude in acoustophoresis microchannels two microfluidic chips were developed, Fig. 3(a). Each chip consists of a straight channel with one inlet and one outlet fabricated using standard photolithography and anisotropic KOH etching in silicon $\langle 100 \rangle$, yielding a rectangular channel cross section. The channel was sealed by an anodically bonded pyrex glass lid, and short pieces of silicone tubing were attached to their respective 1-mm-diameter holes in the glass lid by silicone glue. All dimensions are given in the figure caption. The width W of the chip can be characterized by the ratio α of the number of acoustic wavelengths in silicon and that of water.

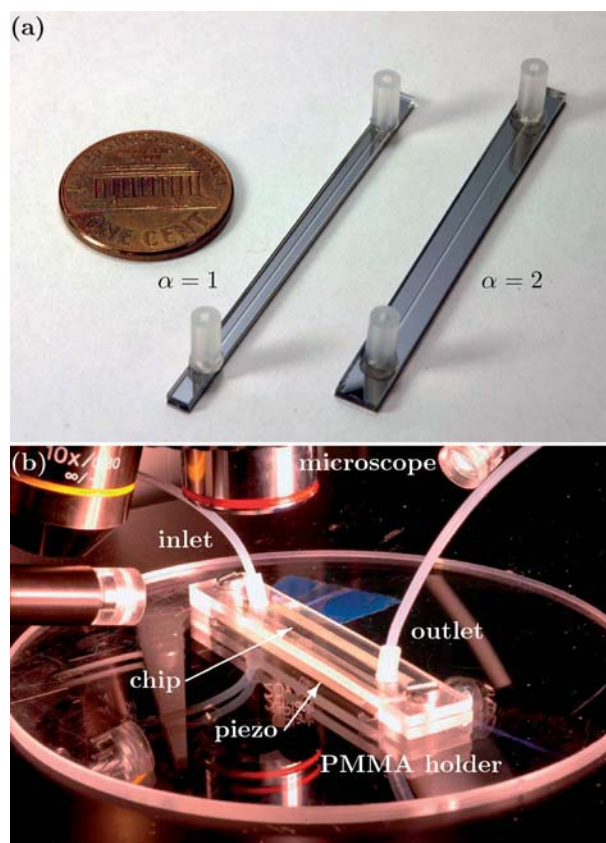


Fig. 3 (a) The silicon/glass chips containing straight channels of length $l = 40$ mm, width $w = 377$ μm , and height $h = 157$ μm . The channels are etched down into the silicon chip of thickness $h_{\text{si}} = 350$ μm , and they are covered by a pyrex glass lid of thickness $h_{\text{py}} = 1.13$ mm. The lengths of the chips are $L = 50$ mm and the widths are $W = 2.52$ mm ($\alpha = 1$) and $W = 4.67$ mm ($\alpha = 2$), respectively. (b) A photograph of the experimental setup with the chip and the PZT piezo crystal mounted under the microscope and the CCD camera. The piezo has the dimension 50.0 mm \times 12.0 mm \times 1.0 mm, and thus the entire chip rests on it.

With the parameters of Table 1 we find $\lambda_{si} = 5.7\lambda_{wa}$ and $\alpha = (W - w)/(5.7w)$. For future experimental purposes we have chosen to fabricate chips with $\alpha = 1$ and $\alpha = 2$.

Fig. 3(b) shows how the chip is mounted on a piezoelectric transducer (piezo) made of hard PZT of the type Pz26 from Ferroperm Piezoceramics A/S. Sufficient acoustic coupling is provided by a thin glycerol layer. The two elements are fixed in a PMMA holder, such that the chip is only in contact with the holder through its inlet/outlet silicone tubing and *via* the piezo, which in turn was mounted so that all contact with the PMMA holder is restricted to its edges.

The piezo is actuated by applying a harmonically oscillating voltage generated from a tone generator, Hewlett Packard 33120A. The voltage is amplified by a T&C Power Conversion Inc. AG Series Amplifier, and the applied peak-to-peak voltage across the piezo transducer is measured by an oscilloscope Tektronix TDS 1002. The channel was monitored through an Olympus BX51WI microscope with an attached CCD camera of the type Infinity 1 from MediaCybernetics.

B. Handling of the microbeads

When carrying out the experiments a liquid suspension of microbeads was injected into the microchannel. The sample liquid consists of Milli-Q water mixed with 0.01% Tween20, a polysorbate surfactant reducing the adhesion of microbeads to the channel walls, and polystyrene microbeads (5.16 ± 0.08 μm from Sigma-Aldrich). The microbead concentrations were in the range from 0.1 g/L to 0.5 g/L. The sample liquid is contained in a 1 mL plastic syringe, in which a small magnet resides. By moving an external magnet, sedimentation of the microbeads inside the syringe is avoided by the stirring, and this reduces the risk of getting an inhomogeneous distribution of microbeads in the microchannel. A syringe pump of the type WPI SP210IWZ was used to purge the microchannel with the sample liquid prior to each run. During all measurements the flow was temporarily stopped.

C. Measuring the Stokes drag force

To investigate the effect of Tween20 in the suspension, repeated recordings were carried out of the sedimentation time of individual microbeads moving from top to bottom of the microchannel. The initial positioning at the lid was achieved by acoustophoresis, which, however, left some microbeads behind, pinned at the channel bottom. We focused the microscope to the microbeads at the lid. These microbeads were then released and followed during their sedimentation by moving the focal plane. The sedimentation was timed from the release until the pinned beads at the bottom appeared in the same focal plane as the sedimenting beads. The sedimentation time for microbeads in Milli-Q water with and without Tween20 (0.01%) was (179 ± 6) s and (182 ± 5) s, respectively. This demonstrates that the influence of the added Tween20 on the density and viscosity is negligible. Moreover, since the theoretical single-microbead sedimentation time calculated from the force balance (neglecting bead-wall interactions) between gravity, buoyancy and Stokes drag is 208 s, our sedimentation measurements also show a fair accuracy in applying the Stokes drag in this confined system.

D. Measuring microbead paths during acoustophoretic focusing

The field of view of the microscope covered the full width $w = 377$ μm of the microchannel, 510 μm along the channel, and it was centered 10 mm downstream from the inlet.

The acoustic energy density was measured by observing the transient acoustophoretic focusing of the microbeads as follows. First, the driving frequency is tuned until observing a strong, resonant, acoustic focusing of the polystyrene microbeads towards the center of the channel. Then the ultrasound field is turned off, and a fresh suspension of microbeads from the syringe pump is injected into the channel. When a homogeneous microbead distribution is observed, the flow is stopped, Fig. 4(a). Finally, the ultrasound is turned back on, and the transient focusing of the microbeads towards the channel center is recorded by the CCD camera, Fig. 4(b). From the frames of the resulting movie we can then determine the transverse paths $y(t)$ of the microbeads, an example of which is shown in Fig. 4(c).

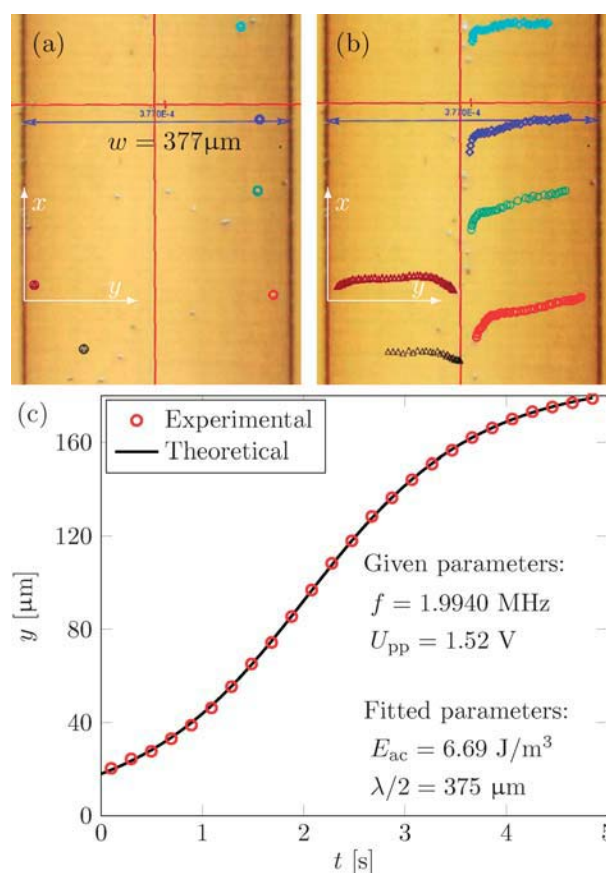


Fig. 4 (a) Starting position (circles) of six microbeads in the channel of the chip with $\alpha = 2$. The channel walls are the two thick vertical lines separated by $w = 377$ μm . (b) Tracking of the paths of the six microbeads. (c) Measurement (circles) for one of the microbeads of its transverse position y from the left wall as a function of time t . The uncertainty in the y -position is 5 μm corresponding to the diameter of the circles. For clarity only every second point is shown, but all points are used in the analysis. The fitted curve (full line) is given by eqn (18) with only two fitting parameters: the acoustic energy density E_{ac} and the half wavelength $\lambda/2$ of the transverse standing pressure wave.

IV. Results

A. Measured acoustic energy density and local pressure amplitude

The transverse path $y(t)$ is extracted from the video recordings by employing the free video analysis tool *Tracker 2.6*.⁴² This software enables tracking of a polystyrene microbead by simple manual mouse-clicking on the microbead position y on each movie frame, for which the time t is known. For a general introduction to tracking techniques of microbeads in microfluidics see ref. 43. The length scale in the y -direction is calibrated by the distance between the visible channel walls as shown in Fig. 4(a). The resulting list of (t, y) -coordinates can be extracted for any tracked microbead path, see Fig. 4(b), and plotted as shown in Fig. 4(c) for a driving frequency of $f = 1.9940$ MHz and a driving voltage $U_{pp} = 1.52$ V.

The axial motion $x(t)$ seen in the last part of the paths shown in Fig. 4(b) is due to hydraulic compliance of the system leading to difficulties in keeping the liquid at complete rest.

Using the energy density E_{ac} and the half-wavelength $\lambda/2$ as the only fitting parameters, a curve of the form $y(t)$ given by eqn (18) is fitted to the data points by the least-squares routine `lsqcurvefit()` in `MATLAB`. As shown by the full curve in Fig. 4(c), this fitting procedure yields good results: the observed path has the theoretically predicted shape, and we can extract reliable values for the acoustic energy density E_{ac} . In the given case we found $E_{ac} = 6.69$ J/m³, and we also note that the fitted value for $\lambda/2$ is 375 μm , very close to the expected value, namely the width of the channel $w = 377$ μm .

From eqn (13) we find the pressure amplitude in the chip with $\alpha = 2$ to be

$$p_a = 2\sqrt{\rho_{wa}c_{wa}^2 E_{ac}} \approx 0.242 \text{ MPa}, \quad (21)$$

which is 10^{-4} times the cohesive energy density 2.6 GPa of water. Equivalently, the density fluctuations are 10^{-4} times ρ_{wa} , and thus the acoustic perturbation theory holds even at resonance.

In our low-voltage experiments we have measured energy densities in the range 0.65–50 J/m³ corresponding to pressure amplitudes in the range 0.08–0.66 MPa. The upper range of these results are consistent with previously reported estimates in the literature for microbead acoustophoresis in microsystems. Using external electric forces, Wiklund *et al.*³⁴ measured energy densities in the range 65–650 J/m³ corresponding to pressure amplitudes in the range 0.76–2.4 MPa, while Hultstöm *et al.*¹⁴ used force balance between gravity and acoustophoretic forces to measure energy densities in the range 37–82 J/m³ corresponding to pressure amplitudes in the range 0.57–0.85 MPa

B. Measured energy density versus driving voltage

In the following we use the above procedure to extract the acoustic energy density E_{ac} and half the wavelength $\lambda/2$ for 5–15 (typically 8) individual microbeads properly chosen in the field of view for any given setting of the external parameters. When plotting the resulting data as a function of the parameters, each data point is a statistical average of these individual measurements, and the error bars are the associated standard deviations.

First, at the driving frequency $f = 1.9976$ MHz, we study the energy density and the half wavelength as a function of the peak-to-peak value U_{pp} of the driving voltage on the piezo transducer in the range from 0.5 V to 1.9 V.

In Fig. 5(a) we see that the resulting ten data points are well fitted to a power law of the form $E_{ac} \propto (U_{pp})^{2.07}$. This is close to a power of 2, which is expected since the acoustic pressure delivered by the piezo transducer is proportional to the applied voltage, and the acoustic energy density is proportional to the square of the pressure, see eqn (21). We also note that the statistically determined error bars increase with increasing driving voltage and thus with increasing microbead velocity. This is as result of the decreased temporal resolution of the paths given the fixed rate of 16 CCD frames per second and the increased microbead velocity.

Fig. 5(b) shows that for all voltages the average of the other fitting parameter, the half wavelength, is $\bar{\lambda}/2 \pm \Delta\lambda = (380 \pm 3)$ μm , which is very close to the expected value of $w = (377 \pm 5)$ μm , the width of the channel.

C. Measured resonance frequencies and Q factors

By measuring the acoustic energy density E_{ac} as a function of the applied frequency f across the piezo transducer, we have been

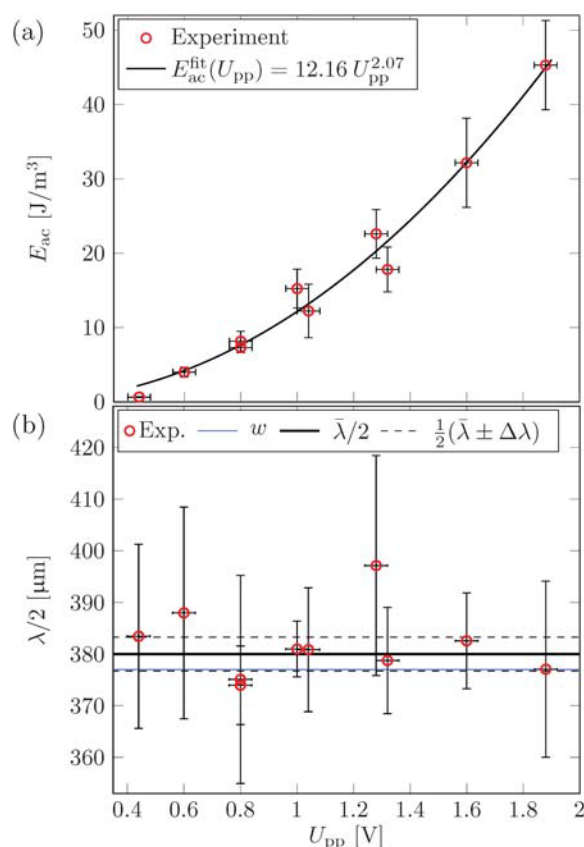


Fig. 5 (a) Measured acoustic energy density E_{ac} versus applied peak-to-peak voltage U_{pp} on the piezo transducer (points) for $\alpha = 1$. A power law fit (full line) to the data is close to the expected square law, $E_{ac} \propto (U_{pp})^2$. (b) The measured half wavelength $\lambda/2$ obtained by the path fitting is independent of U_{pp} , and its average value $\bar{\lambda}/2 = 380$ μm (thick black line) differs less than one standard deviation $\Delta\lambda/2 = 3$ μm (dashed lines) from the expected value of $w = 377$ μm (thin blue line).

able to characterize the acoustic resonances in more detail. The following results were obtained on the chip $\alpha = 2$ of width $W = 4.67$ mm, see Fig. 3(a). The driving frequency f was varied from 1.9900 MHz to 2.0100 MHz, while the tone generator and the amplifier were set to fixed values. However, due to the piezoelectric coupling of the transducer, the actual peak-to-peak voltage U_{pp} varied between 1.44 V and 1.60 V as a function of frequency. We used the quadratic dependency of E_{ac} on U_{pp} , as derived in Fig. 5(a), to correct all measured values of E_{ac} to correspond to the same average voltage 1.48 V.

The measured acoustic energy spectrum $E_{ac}(f)$ is shown in Fig. 6. A clear maximum is seen at $f_2 = 2.0021$ MHz while a smaller, less pronounced peak is seen at $f_1 = 1.9927$ MHz. According to eqn (20), a simple acoustic resonance can be described by a Lorentzian line shape, and we therefore fit the measured spectrum by the sum of two Lorentzian line shapes. In this case we thus end up with six fitting parameters, three per peak, the energy density maxima $E_{ac,1}$ and $E_{ac,2}$, the resonance frequencies f_1 and f_2 , and the Q factors Q_1 and Q_2 . The values of these parameters are listed in the caption of Fig. 6, and from the energy densities we extract as in eqn (21) the pressure amplitudes $p_{a,1} = 0.16$ MPa and $p_{a,2} = 0.37$ MPa for peak 1 and 2 respectively.

The two resonance peaks in Fig. 6 are separated by a spacing $\Delta f_{12} = f_2 - f_1 = 9.4$ kHz, while the line widths of the two peaks are of the same order of magnitude, namely $\delta f_1 = 3.5$ kHz and $\delta f_2 = 9.6$ kHz. These values emphasize, as is also seen directly on the graph, that the individual acoustic resonances are barely resolved.

The origin of the observed two-peak structure is explained qualitatively by the 2D pressure eigenmode simulations shown in Fig. 7. It is seen how axial modes appear and gives rise to closely-lying resonances. While our non-shear-wave model does not allow for accurate determination of these resonance frequencies,

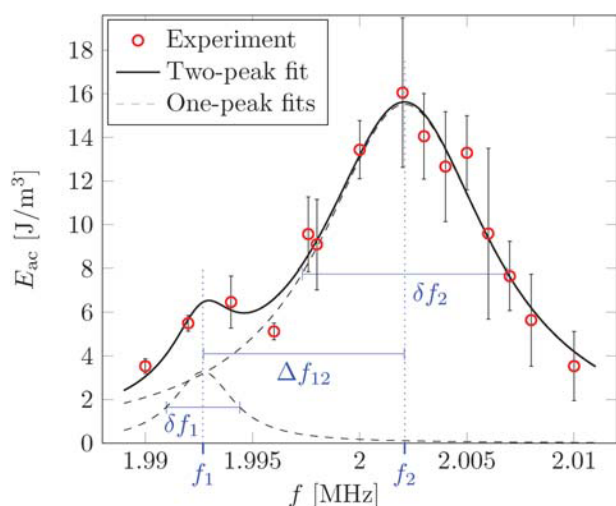


Fig. 6 Measured acoustic energy density E_{ac} versus applied frequency f on the piezo transducer (circles) for the $\alpha = 2$ chip for $U_{pp} = 1.48$ V. The data points are fitted by a sum (full line) of two Lorentzian peaks (dashed lines). The values of the fitting parameters for peak 1 are $f_1 = 1.9927$ MHz, $E_{ac,1} = 3.3$ J/m³, and $Q_1 = 577$. For peak 2 they are $f_2 = 2.0021$ MHz, $E_{ac,2} = 15.5$ J/m³, and $Q_2 = 209$. The peak spacing is $\Delta f_{12} = f_2 - f_1 = 9.4$ kHz, while the line widths are $\delta f_1 = 3.5$ kHz and $\delta f_2 = 9.6$ kHz.

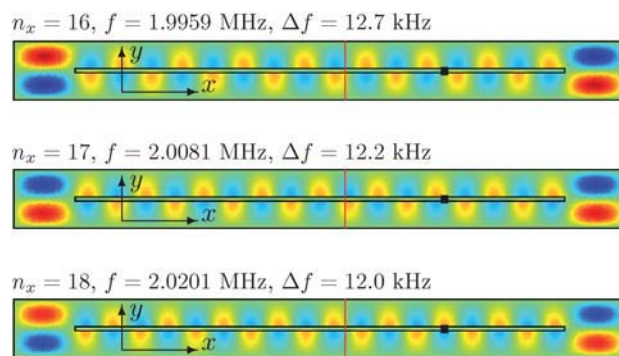


Fig. 7 A top view color plot (blue negative, red positive) of the pressure field of three ultrasound resonances calculated in a simplified 2D model. For each resonance is shown the number of n_x of half wavelengths in the axial direction, the resonance frequency f , and the distance Δf in frequency space to the neighboring resonance. The small black rectangles mark the microscope field of view.

it nevertheless provides a reliable order-of-magnitude estimate for the spacing between them, $\Delta f \approx 12$ kHz, close to the observed $\Delta f_{12} = 9.4$ kHz. Furthermore, we speculate that the difference in amplitude between the two peaks shown in Fig. 6 is mainly due to the shift in wave pattern going from one value n_x to the neighboring peak at $n_x + 1$ as illustrated by black rectangles in Fig. 7, representing the microscope field of view. For $n_x = 17$ the pressure amplitude in the field of view is much smaller than that for $n_x = 18$. We note that for $n_x = 17$ the k -related angle θ , see eqn (11), becomes 81° , corresponding to $\sin^2 \theta = 0.98$ and $\cos^2 \theta = 0.02$. According to eqn (14) this fully determines the position dependence of the acoustic energy density. For more details on axial modes see ref. 38.

V. Concluding discussion

We have established a new method to measure *in situ* the energy density, the local pressure amplitude, and the Q factor of ultrasound resonances in microfluidic chips by tracking individual polystyrene microbeads undergoing acoustophoresis in straight water-filled channels in silicon/glass chips. For a given driving frequency and voltage amplitude of the piezo transducer, microbead tracks have been recorded by a CCD camera and fitted to a theoretical curve. From the curve fit we have obtained the acoustic energy density and pressure amplitude. We have shown that, as expected, the acoustic energy density scales with applied piezo voltage to the power 2. Furthermore, by plotting the energy densities as a function of the applied ultrasound frequency, we obtain Lorentzian line shapes, from which we can determine the resonance frequency and the Q factor for each acoustic resonance peak.

In contrast to previous methods, our method to determine the local pressure amplitude in microchannel acoustophoresis has the advantage of relying only on the acoustophoretic effect itself and not on calibration against external forces. Moreover, being based on particle tracking, it provides the means to measure very low pressure levels with high accuracy, here down to 0.08 MPa at $U_{pp} = 0.44$ V. Equipped with high-speed CCD cameras faster than our present 16 frames/s, our method is easily extendable to pressure levels above the 0.66 MPa reported here.

The work presented here shows one example of how the new characterization methods may lead to improvements. In Fig. 6 it is shown that the nearest-neighbor resonances are separated by $\Delta f_{12} = 9.4$ kHz, while the line width of the two peaks are of the same order of magnitude, namely $\delta f_1 = 3.5$ kHz and $\delta f_2 = 9.6$ kHz. Thus, for this standard setup, the acoustic resonances are barely resolved due to line widening from loss of acoustic energy from the resonating system. In future work, especially work involving actuation of several frequencies simultaneously or sequentially as in ref. 16 and 44, it is therefore desirable to focus on reducing the acoustic energy loss by a more careful design of the coupling between the chip and the surroundings, in particular regarding the piezo transducer and the fluidic tubing.

In general, our new method paves the way for improved design of lab-on-a-chip systems using acoustophoresis. Once fully automated by computer control of the particle tracking and the subsequent curve fitting, detailed *in situ* characterization of the entire acoustic pressure field in microchannel acoustophoresis will become feasible. Acquisition of such detailed data will be beneficial both for further studies of the fundamental physical nature of acoustophoresis and acoustic streaming, and for improved engineering of chip-based systems.

Acknowledgements

This research was supported by the Danish Council for Independent Research, Technology and Production Sciences, Grant No. 274-09-0342; the Swedish Research Council, Grant No. 2007-4946; and the Swedish Governmental Agency for Innovation Systems, VINNOVA, the programme Innovations for Future Health, Cell CARE, Grant No. 2009-00236.

References

- 1 L. V. King, *Proc. R. Soc. London, Ser. A*, 1934, **147**, 212.
- 2 K. Yosioka and Y. Kawasima, *Acustica*, 1955, **5**, 167.
- 3 L. P. Gorkov, *Sov. Phys. Doklady*, 1962, **6**, 773.
- 4 K. Yasuda, S. Umemura and K. Takeda, *Jpn. J. Appl. Phys.*, 1995, **34**, 2715.
- 5 H. Gröschl, W. Burger and B. Handl, *Acustica*, 1998, **84**, 815.
- 6 J. Hawkes and W. T. Coakley, *Enzyme Microb. Technol.*, 1996, **19**, 57.
- 7 J. Hawkes and W. T. Coakley, *Sens. Actuators, B*, 2001, **75**, 213–222.
- 8 H. Nilsson, M. Wiklund, T. Johansson, H. M. Hertz and S. Nilsson, *Electrophoresis*, 2001, **22**, 2384.
- 9 T. Laurell, F. Petersson and A. Nilsson, *Chem. Soc. Rev.*, 2007, **36**, 492.
- 10 J. Nilsson, M. Evander, B. Hammarström and T. Laurell, *Anal. Chim. Acta*, 2009, **649**, 141–157.
- 11 T. Lilliehorn, U. Simu, M. Nilsson, M. Almqvist, T. Stepinski, T. Laurell, J. Nilsson and S. Johansson, *Ultrasonics*, 2005, **43**, 293.
- 12 D. Bazou, L. A. Kutznetsova and W. T. Coakley, *Ultrasonics Med. Biol.*, 2005, **31**, 423.
- 13 M. Evander, L. Johansson, T. Lilliehorn, J. Piskur, M. Lindvall, S. Johansson, M. Almqvist, T. Laurell and J. Nilsson, *Anal. Chem.*, 2007, **79**, 2984.
- 14 J. Hultström, O. Manneberg, K. Dopf, H. M. Hertz, H. Brismar and M. Wiklund, *Ultrasonics Med. Biol.*, 2007, **33**, 145.
- 15 O. Manneberg, B. Vanherberghen, J. Svennebring, H. M. Hertz, B. Önfelt and M. Wiklund, *Appl. Phys. Lett.*, 2008, **93**, 063901.
- 16 J. Svennebring, O. Manneberg, P. Skafte-Pedersen, H. Bruus and M. Wiklund, *Biotechnol. Bioeng.*, 2009, **103**, 323.
- 17 N. R. Harris, M. Hill, S. Beeby, Y. Shen, N. M. White, J. J. Hawkes and W. T. Coakley, *Sens. Actuators, B*, 2003, **95**, 425.
- 18 M. Bengtsson and T. Laurell, *Anal. Bioanal. Chem.*, 2004, **378**, 1716.
- 19 J. J. Hawkes, R. W. Barber, D. R. Emerson and W. T. Coakley, *Lab Chip*, 2004, **4**, 446.
- 20 A. Nilsson, F. Petersson, H. Jonsson and T. Laurell, *Lab Chip*, 2004, **4**, 131.
- 21 F. Petersson, A. Nilsson, C. Holm, H. Jönsson and T. Laurell, *Analyst*, 2004, **129**, 938.
- 22 F. Petersson, A. Nilsson, H. Jönsson and T. Laurell, *Anal. Chem.*, 2005, **77**, 1216.
- 23 F. T. Petersson, L. B. Åberg, A.-M. S. Swärd-Nilsson and T. Laurell, *Anal. Chem.*, 2007, **79**, 5117.
- 24 J. Persson, P. Augustsson, T. Laurell and M. Ohlin, *FEBS J*, 2008, **275**, 5657.
- 25 O. Manneberg, S. M. Hagsäter, J. Svennebring, H. M. Hertz, J. P. Kutter, H. Bruus and M. Wiklund, *Ultrasonics*, 2009, **49**, 112.
- 26 C. Grenvall, P. Augustsson, J. R. Folkenberg and T. Laurell, *Anal. Chem.*, 2009, **81**, 6195.
- 27 H. Nowotny and E. Benes, *J. Acoust. Soc. Am.*, 1987, **82**, 513.
- 28 M. Hill and R. J. K. Wood, *Ultrasonics*, 2000, **38**, 662.
- 29 J. J. Hawkes, W. T. Coakley, M. Gröschl, E. Benes, S. Armstrong and P. J. Tasker, *J. Acoust. Soc. Am.*, 2002, **111**, 1259.
- 30 M. Hill, Y. Shen and J. J. Hawkes, *Ultrasonics*, 2002, **40**, 385.
- 31 M. Hill, *J. Acoust. Soc. Am.*, 2003, **114**, 2654.
- 32 S. M. Hagsäter, T. G. Jensen, H. Bruus and J. P. Kutter, *Lab Chip*, 2007, **7**, 1336.
- 33 S. M. Hagsäter, A. Lenshof, P. Skafte-Pedersen, J. P. Kutter, T. Laurell and H. Bruus, *Lab Chip*, 2008, **8**, 1178.
- 34 M. Wiklund, P. Spéjel, S. Nilsson and H. M. Hertz, *Ultrasonics*, 2003, **41**, 329.
- 35 J. Lighthill, *Waves in fluids*, Cambridge University Press, Cambridge, 2005.
- 36 H. Bruus, *Theoretical Microfluidics*, Oxford University Press, Oxford, 2008.
- 37 M. Barmatz and P. Collas, *J. Acoust. Soc. Am.*, 1985, **77**, 928.
- 38 R. Barnkob and H. Bruus, *Proceedings of Meetings on Acoustics*, 2009, **6**, 020001, DOI: 10.1121/1.3186746, 15.
- 39 W. L. Nyborg, *Ultrasonics: Its Applications in Medicine and Biology*, ed. F. J. Fry, Elsevier, New York, 1978, Part 1, pp. 1–76.
- 40 R. J. Townsend, M. Hill, N. R. Harris and N. M. White, *Ultrasonics*, 2004, **42**, 319.
- 41 M. S. Limaye and W. T. Coakley, *J. Appl. Microbiol.*, 1998, **84**, 1035.
- 42 D. Brown. Tracker 2.60, *Free video analysis and modeling tool for physics education. Online open source*: <http://www.cabrillo.edu/dbrown/tracker/>, April 2009.
- 43 M. Raffel, C. E. Willert, S. T. Wereley, and J. Kompenhans, *Particle Image Velocimetry, A Practical Guide*, 2nd edn, Springer Verlag, Berlin, 2007.
- 44 O. Manneberg, B. Vanherberghen, B. Önfelt and M. Wiklund, *Lab Chip*, 2009, **9**, 833.